metals

MDPI

Article

First-Principles Study on the Adsorption Characteristics of Corrosive Species on Passive Film TiO_2 in a NaCl Solution Containing H_2S and CO_2

Pan Dong [1], Yanna Zhang [2], Shidong Zhu [1,*], Zhen Nie [2], Haixia Ma [3], Qiang Liu [4] and Jinling Li [5]

1 School of Materials Science and Engineering, Xi'an Shiyou University, Xi'an 710065, China; dongp0813@126.com
2 Middle East E&P, Research Institute of Petroleum Exploration & Development, Beijing 100083, China; zhangyanna@petrochina.com.cn (Y.Z.); niezhen@petrochina.com.cn (Z.N.)
3 School of Chemical Engineering, Northwest University, Xi'an 710069, China; mahx@nwu.edu.cn
4 State Key Laboratory for Performance and Structure Safety of Petroleum Tubular Goods and Equipment Materials, CNPC Tubular Goods Research Institute, Xi'an 710077, China; liuqiang030@cnpc.com.cn
5 College of Chemistry & Chemical Engineering, Xi'an Shiyou University, Xi'an 710065, China; lijinling@xsyu.edu.cn
* Correspondence: zhusdxt@126.com; Tel.: +86-29-88382598

Abstract: The adsorption characteristics of corrosive anions (Cl^-, HS^-, S^{2-}, HCO_3^- and CO_3^{2-}) on TiO_2 of TC4 titanium alloy in a NaCl solution containing H_2S and CO_2 were studied by density functional theory (DFT). The stable adsorption configuration of each corrosive species on the TiO_2 (110) surface was obtained by geometric optimization, and the electronic structure and interface binding energy were calculated and analyzed. The results showed that the optimal adsorption positions of Cl^-, HS^-, S^{2-}, HCO_3^- and CO_3^{2-} on TiO_2 (110) were all bridge positions. There was a strong charge interaction between the negatively charged Cl, S and O atoms in Cl^-, HS^-, S^{2-}, HCO_3^- and CO_3^{2-} and the positively charged Ti atoms of TiO_2. The interface bonding was mainly caused by charge movement from around Ti atoms to around Cl, O, S atoms. The energy levels were mainly caused by the electron orbital hybridization of Cl-3p^5, S-3p^4, O-2p^4 and Ti-3d^2. All adsorption configurations were chemical adsorption. The order of influence of the five ions on the stability of TiO_2 was $S^{2-} > CO_3^{2-} > Cl^- > HS^- > HCO_3^-$. Finally, a novel corrosion mechanism was proposed to illustrate the dynamic evolution processes of pits.

Keywords: titanium alloy; passive film; first-principles; adsorption characteristic; interface stability

check for updates

Citation: Dong, P.; Zhang, Y.; Zhu, S.; Nie, Z.; Ma, H.; Liu, Q.; Li, J. First-Principles Study on the Adsorption Characteristics of Corrosive Species on Passive Film TiO_2 in a NaCl Solution Containing H_2S and CO_2. *Metals* **2022**, *12*, 1160. https://doi.org/10.3390/met12071160

Academic Editor: Alexandre Emelyanenko

Received: 15 June 2022
Accepted: 5 July 2022
Published: 7 July 2022

1. Introduction

In the process of oil and gas exploitation and transportation, corrosive media such as H_2S, CO_2 and Cl^- are often encountered, oil country tubular goods (OCTGs) will suffer from corrosion, which is sometimes serious, and the cost of corrosion is increasing daily [1]. According to statistics, the consumption of the petroleum industry is approximately CNY 10 billion for OCTG every year in China, and most of these expenses are caused by corrosion [2,3]. With the rapid development of the petroleum industry, drilling conditions are becoming increasingly severe. The common materials used in oil and gas fields, such as carbon steel and conventional stainless steel, have been unable to meet the needs for the technical development of modern drilling and the extraction and transportation of oil and gas [4–6].

Titanium alloy has been widely used in many fields because of its high strength-to-weight ratio, its excellent mechanical properties and its good corrosion resistance [7–15]; among them, the excellent corrosion resistance is attributed to the spontaneous oxide passive film (TiO_2) on the surface of titanium alloy [16,17]. The stability of the passive

film on the surface of titanium alloy exposed to the working environment depends on its electronic properties, which are closely related to the electrochemical reactivity and the redox reaction at the metal/oxide interface [9].

The passive film on titanium alloy is only a few nanometers thick, and the adsorption characteristics of corrosive species such as Cl^-, HS^- and HCO_3^- on the surface of corrosion-resistant alloys have only been studied on a limited basis. Therefore, it is difficult to study the thermodynamic stability of the interface between the passive film and the solution and to further study the electronic structure, bonding type and bonding strength after adsorption on the surface of passive film only by experimental means. First-principles calculations, especially the density functional theory (DFT) method, can link the microscopic properties of metal materials with their structural and thermodynamic properties, providing a powerful tool for the study of adsorption systems [18]. Fu [19] found that the adsorption capacity of H_2S at the top and bridge positions on the Mo_2C (001) surface was also weak, with adsorption energies of 23.23 kcal/mol and 26.12 kcal/mol, respectively. Lin [20] believed that when CO molecules were adsorbed on the surface of SiC (111), the adsorption of O atoms in CO molecules in the vertical direction of Si atoms was the most stable, and the adsorption energy was −1.24 eV. Lin [21] argued that there was almost no charge transferred from the SiC (111) surface to the CH_4 molecule during the adsorption of CH_4 on the SiC (111) surface, and it could be seen that the adsorption mechanism was physical adsorption based on the diagram of the electron density difference and the density of states.

Therefore, the adsorption characteristics (electronic structure and interfacial binding energy) of corrosive ions (Cl^-, HS^-, S^{2-}, HCO_3^- and CO_3^{2-}) on the passive film (TiO_2) of TC4 titanium alloy were investigated by using the CASTEP module in the first-principles Materials Studio simulation software based on density functional theory, and the thermodynamic stability characteristics of the passive film interface on TC4 titanium alloy were obtained. Finally, the corrosion resistance mechanism of TC4 titanium alloy in a harsh corrosion environment (CO_2-H_2S-Cl^- medium system) was revealed from the micro perspective to provide a theoretical basis for the development of titanium alloy and its applicability in oil and gas fields.

2. Modeling and Computing

TiO_2 is a metal oxide semiconductor with polycrystalline properties [22], and it has three types of crystalline structures: rutile, anatase and brookite. They are all composed of octahedral structures, but their arrangement, linkage and lattice structure are different [23]. Rutile TiO_2 belongs to the tetragonal crystal system structure, and its space group is P42/MNM [24], as shown in Figure 1a, around which each octahedron is connected to ten octahedrons, with two common edges and eight common apex angles. Each protocell consists of two TiO_2 molecules, and thus, the molecular formula is Ti_2O_4. Anatase TiO_2 belongs to the tetragonal crystal system structure, as shown in Figure 1b. Each octahedron is connected to eight octahedrons, with four common sides and four common apical angles. Each primitive cell consists of four TiO_2 molecules, and thus, the molecular formula is Ti_4O_8. Brookite TiO_2 belongs to the orthorhombic crystal system, as shown in Figure 1c. Each primitive cell consists of six TiO_2 molecules, and thus, the molecular formula is Ti_6O_{12}.

The rutile phase is stable under atmospheric conditions and is also the main component phase of passive films on titanium alloys. Burnside and Labat [25,26] simulated the relative energy of rutile TiO_2 (110), (100) and (001) crystal faces and found that the relative energy of the TiO_2 (110) crystal face was the lowest and most stable. Studies have shown that the (110) crystal face of TiO_2 was the close-packed surface and the thermodynamically stable surface with the lowest energy [27,28]. Zhao [29] also obtained that the rutile phase characteristic peak was the (110) face by XRD analysis and found that the 0.320 nm lattice fringes shown in the sample correspond to the (110) face of the rutile phase through HR-TEM. Therefore, the (110) crystal face of rutile TiO_2 was selected for the first-principles calculation in this paper.

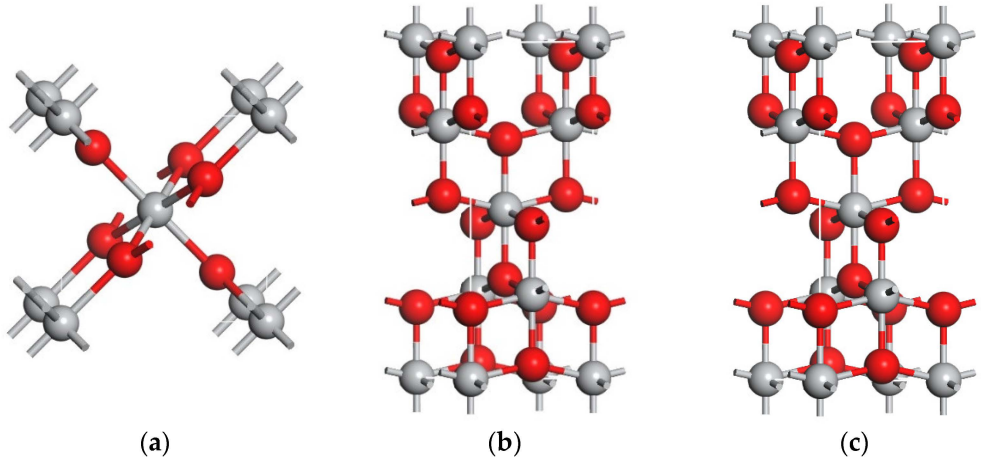

Figure 1. The crystal structure of TiO_2 (light gray atoms represent Ti; red atoms represent O): (**a**) rutile TiO_2; (**b**) anatase TiO_2; (**c**) brookite TiO_2.

2.1. Modeling

The interface characteristics of all the adsorption models were calculated by the CASTEP module based on density functional theory (DFT) in Material Studio software [30,31]. Taking full account of the degree of conformity with the actual situation, the actual calculation strength of the server and the calculation requirements of CASTEP, the supercell structure of the TiO_2 (110) face in three-dimensional space with $2 \times 1 \times 1$ periodic boundary conditions was established. To avoid the interaction between the plates, a vacuum region of 15 Å was added between the plates. Figure 2 shows the interface models of different corrosive species (Cl^-, HS^-, S^{2-}, HCO_3^- and CO_3^{2-}) at three adsorption positions (top, bridge and hole) on the TiO_2 (110) crystal face.

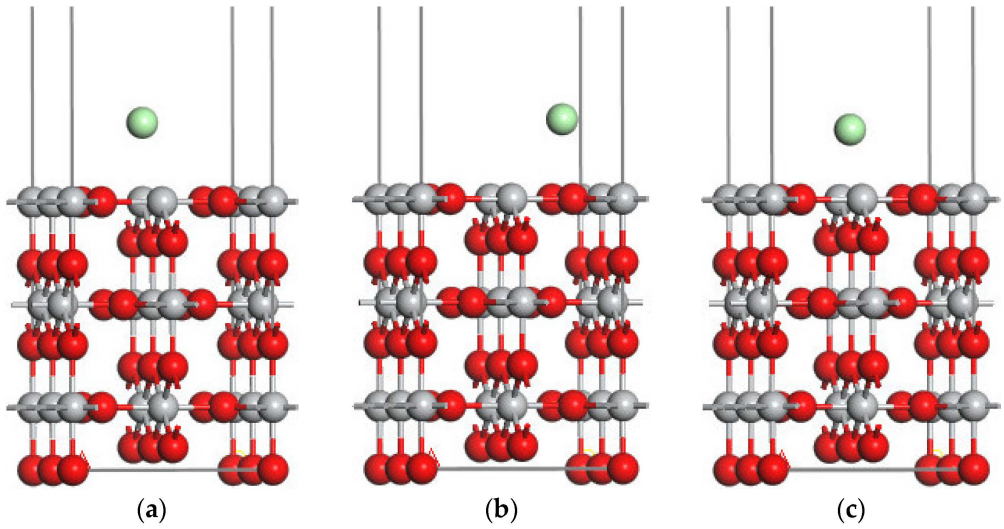

Figure 2. *Cont.*

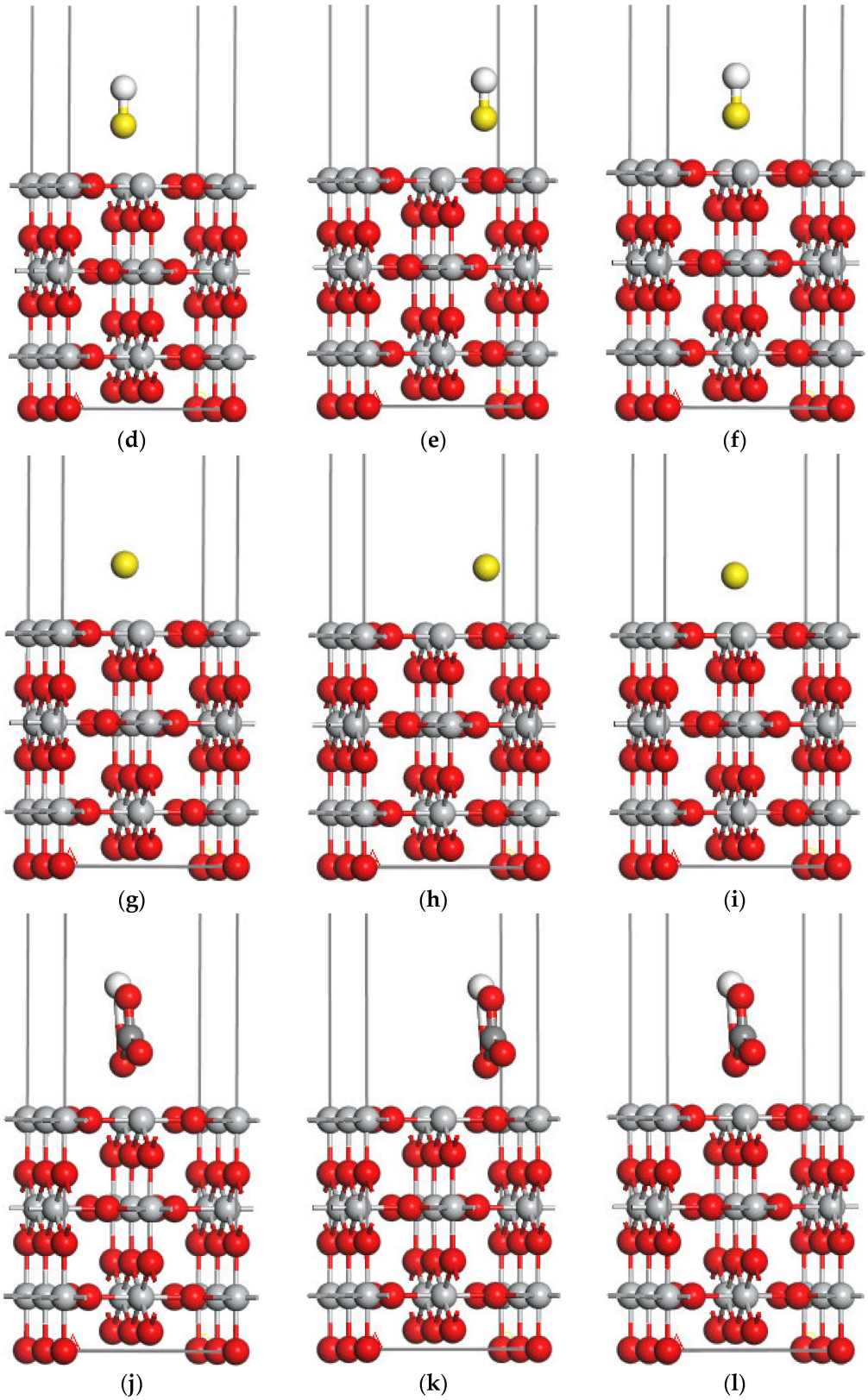

Figure 2. *Cont.*

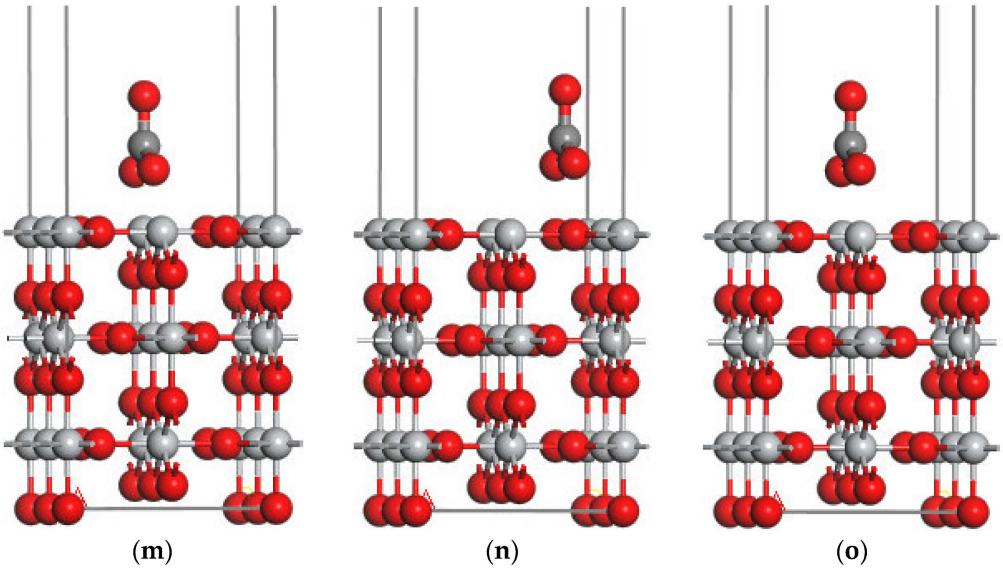

Figure 2. Interface model of TiO_2 (110) containing different corrosive species: (**a**) TiO_2 (top)—Cl^-; (**b**) TiO_2 (bridge)—Cl^-; (**c**) TiO_2 (hole)—Cl^-; (**d**) TiO_2 (top)—HS^-; (**e**) TiO_2 (bridge)—HS^-; (**f**) TiO_2 (hole)—HS^-; (**g**) TiO_2 (top)—S^{2-}; (**h**) TiO_2 (bridge)—S^{2-}; (**i**) TiO_2 (hole)—S^{2-}; (**j**) TiO_2 (top)—HCO_3^-; (**k**) TiO_2 (bridge)—HCO_3^-; (**l**) TiO_2 (hole)—HCO_3^-; (**m**) TiO_2 (top)—CO_3^{2-}; (**n**) TiO_2 (bridge)—CO_3^{2-}; (**o**) TiO_2 (hole)—CO_3^{2-}.

2.2. Computational Methods

The PBE functional form under the generalized gradient approximation (GGA) was used for all calculations, and the ultrasoft pseudopotential self-consistent field (SCF) was used to construct the pseudopotential [32–34]. The plane wave cutoff energy was 425 eV, and the self-consistent iteration was 500 times. The convergence accuracy was 2×10^{-6} eV/atom, the force converged to 0.03 eV/atom, the stress deviation was less than 0.08 GPa, the tolerance deviation was less than 0.005 and the value of the *k* point in the Brillouin zone was $4 \times 4 \times 1$.

3. Results and Discussion

3.1. Optimum Structure and Stable Adsorption Configuration

(1) Optimum structure

Table 1 is a comparison of the lattice constants of the rutile TiO_2 in this paper to those in the literature [35]. The errors of "a" and "c" were only ±0.02% and ±0.07%, respectively, indicating that the constructed model conformed to the actual requirements.

Table 1. Comparison of the lattice constants of rutile TiO_2 between the calculated values and the literature values.

Lattice Constant	Calculated Value/Å	Literature Value/Å	Error/%
a	4.5940	4.5930	±0.02
c	2.9590	2.9610	±0.07
c/a	0.6441	0.6447	±0.09

(2) Stable adsorption configuration

Since each atom in the nonrelaxation state of TiO_2 is fixed, it is equivalent to the mechanical accumulation in a specific position. However, the atoms in the relaxation state of TiO_2 can move within the crystal cell. After the geometric optimization of the adsorption structures with corrosive species adsorbed on the surface of TiO_2, an optimal position was needed, in which the energy of the system was the lowest—that is, the system was the most stable at this time. Therefore, the geometries of all adsorption positions were optimized to select the most stable adsorption configuration. Table 2 shows the final energies of Cl^-,

HS^-, S^{2-}, HCO_3^- and CO_3^{2-} at each adsorption position (top, bridge and hole) on the TiO_2 (110) crystal face after geometric optimization.

Table 2. The final energy of each corrosive species at each adsorption position on the TiO_2 (110) crystal face after geometric optimization.

Model	Final Energy/eV
TiO_2 (top)—Cl^-	−30,176.98682254
TiO_2 (bridge)—Cl^-	−30,177.36115795
TiO_2 (hole)—Cl^-	−30,177.35786327
TiO_2 (top)—HS^-	−30,061.99607022
TiO_2 (bridge)—HS^-	−30,062.32529929
TiO_2 (hole)—HS^-	−30,062.32232474
TiO_2 (top)—S^{2-}	−30,045.12435310
TiO_2 (bridge)—S^{2-}	−30,045.13031885
TiO_2 (hole)—S^{2-}	−30,045.12848408
TiO_2 (top)—HCO_3^-	−31,247.50645571
TiO_2 (bridge)—HCO_3^-	−31,250.09178742
TiO_2 (hole)—HCO_3^-	−31,249.39763267
TiO_2 (top)—CO_3^{2-}	−31,233.00592263
TiO_2 (bridge)—CO_3^{2-}	−31,233.01017140
TiO_2 (hole)—CO_3^{2-}	−31,233.00957590

The final energies of Cl^-, HS^-, S^{2-}, HCO_3^- and CO_3^{2-} at the bridge position on the TiO_2 (110) crystal face were the lowest; the lower the total cell energy is, the more stable the cell structure is [36]. Therefore, the optimal adsorption positions of Cl^-, HS^-, S^{2-}, HCO_3^- and CO_3^{2-} on the TiO_2 (110) surface were all bridge positions, and the final energy order of the corrosive species at the bridge position on the TiO_2 (110) crystal face was $S^{2-} > HS^- > Cl^- > CO_3^{2-} > HCO_3^-$.

3.2. Electron Density

Figure 3 shows the charge density distributions of Cl^-, HS^-, S^{2-}, HCO_3^- and CO_3^{2-} at the bridge position on the TiO_2 (110) crystal face, which can directly reflect the bonding characteristics between atoms [37].

As shown in Figure 3, when the adsorption of corrosive species on the TiO_2 (110) surface reached a stable state, there was a strong charge interaction between the Cl atoms in Cl^-, the S atoms in HS^-, the S atoms in S^{2-}, the O atoms in HCO_3^-, the O atoms in CO_3^{2-} and the Ti atoms on TiO_2 [38]. The red region represents a large density of electrons, which is an active region available for chemical reactions. The deeper the color of the red, the larger the charge density [39]. Interface bonding [40] mainly occurred between the negatively charged atoms in the anion and the positively charged Ti atoms in the TiO_2 (110) crystal face.

Table 3 shows the charge number of the negatively charged atoms in each corrosive species. The absolute value order of the charge number of Cl atoms in the Cl^-, S atoms in HS^-, the S atoms in S^{2-}, the O atoms in HCO_3^- and the O atoms in CO_3^{2-} was $S^{2-} > CO_3^{2-} > Cl^- > HS^- > HCO_3^-$. The charge density represents the number of valence electrons in a volume of pure physical space, and the larger the charge density is, the easier the ions are adsorbed on the metal surface, resulting in the stronger corrosive effect of the ions on the passive film. Therefore, the stability of TiO_2 in the medium containing S^{2-} was the worst, followed by CO_3^{2-}, Cl^-, HS^- and HCO_3^-.

Table 3. Charge number of atoms with a negative charge in each corrosive species.

Atom	Cl^- (Cl)	HS^- (S)	S^{2-} (S)	HCO_3^- (O)	CO_3^{2-} (O)
Charge/e	−0.20	−0.17	−0.41	−0.14	−0.22

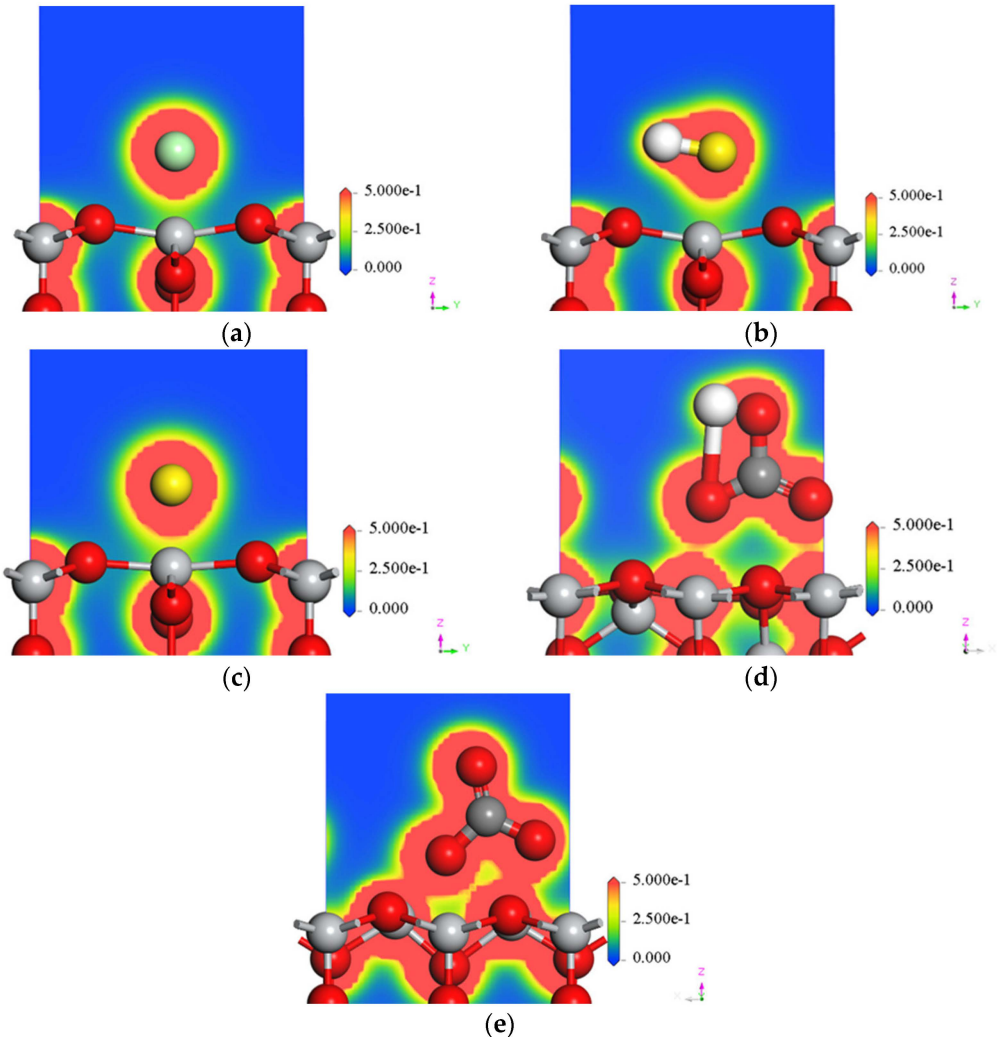

Figure 3. Charge density distribution of corrosive species at the bridge position on the TiO_2 (110) surface: (**a**) Cl^-; (**b**) HS^-; (**c**) S^{2-}; (**d**) HCO_3^-; (**e**) CO_3^{2-}.

3.3. Electron Density Difference

The electron density difference can verify the relevant conclusions of the charge density diagram and more intuitively observe the charge transfer before and after adsorption [41] and the bonding situation [42]. The analysis of the electron density difference was conducted on the steady-state adsorption configuration of Cl^-, HS^-, S^{2-}, HCO_3^- and CO_3^{2-} adsorbed at the crystal plane bridge position of TiO_2 (110), as shown in Figure 4.

When the adsorption of corrosive species on the TiO_2 (110) surface reached a stable state, there was an obvious charge transfer phenomenon between the Cl atoms in Cl^-, the S atoms in HS^-, the S atoms in S^{2-}, the O atoms in HCO_3^-, the O atoms in CO_3^{2-} and the Ti atoms on the surface of TiO_2. In addition, the charge accumulation and electronegativity around the negatively charged atoms in the species decreased, while the charge dissipation and electronegativity around the Ti atoms increased. The interface bonding mainly existed between the Cl atoms in Cl^-, the S atoms in HS^-, the S atoms in S^{2-}, the O atoms in HCO_3^-, the O atoms in CO_3^{2-} and the Ti atoms. The bonding was mainly caused by the charge moving from around the Ti atom to around the Cl atom in Cl^-, the S atom in HS^-, the S atom in S^{2-}, the O atoms in HCO_3^- and the O atoms in CO_3^{2-}.

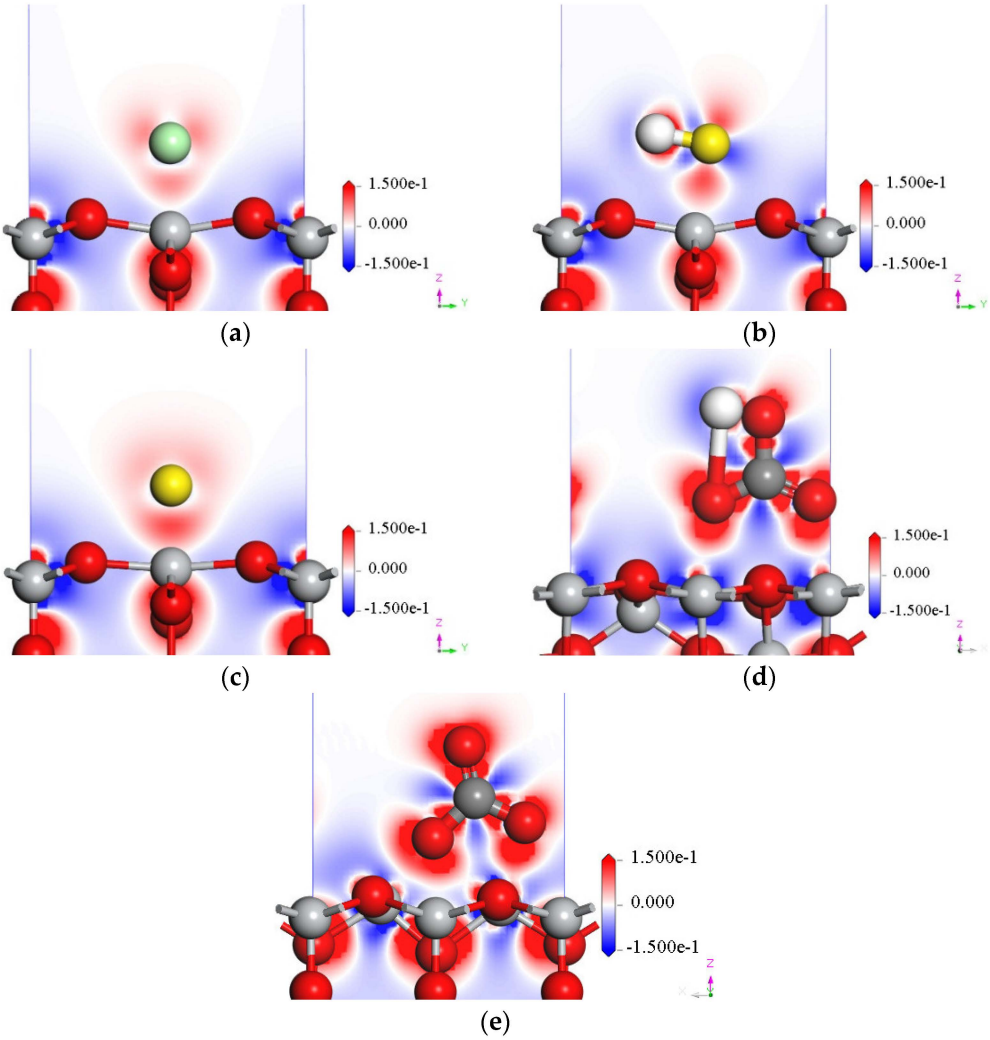

Figure 4. Electron density difference distribution of corrosive species at the bridge position on the TiO_2 (110) crystal face: (**a**) Cl^-; (**b**) HS^-; (**c**) S^{2-}; (**d**) HCO_3^-; (**e**) CO_3^{2-}.

3.4. Density of States

The electron transfer of the interaction between atoms mainly occurs with the valence electrons of each atom. To further investigate the nature of electronic interactions in interface bonding after adsorption and understand the contribution of the electrons of each element to the total density of states of the alloy [43], partial density of states (PDOS) analysis of the steady-state adsorption configurations of Cl^-, HS^-, S^{2-}, HCO_3^- and CO_3^{2-} at the bridge position of the TiO_2 (110) crystal face was carried out, as shown in Figure 5.

Figure 5 shows that there was a certain degree of charge interaction between the Cl atoms in Cl^-, the S atoms in HS^-, the S atoms in S^{2-}, the O atoms in HCO_3^- and the O atoms in CO_3^{2-} with the Ti atoms on the surface of TiO_2, indicating that the adsorption processes were all chemisorption [44]. The charge interactions took place near −6 eV and 0.5 eV~1.5 eV, 0.5 eV~1.5 eV, −6 eV and 0.5 eV, 1 eV, −10.5 eV and −6 eV and 0.5 eV, respectively, which were mainly formed by the hybrid orbitals between the $3d^2$ electrons of Ti and the $3p^5$ electrons of Cl, the $3p^4$ electrons of S and the $2p^4$ electrons of the O atoms. Therefore, after the adsorption of Cl^-, HS^-, S^{2-}, HCO_3^- and CO_3^{2-} on the TiO_2 (110) crystal surface, the interface bonding was mainly caused by the electronic orbital hybridization of Cl-$3p^5$, S-$3p^4$, O-$2p^4$ and Ti-$3d^2$, and the bonding energy levels of the Cl^-, HS^-, S^{2-}, HCO_3^- and CO_3^{2-} ions were mainly located near the corresponding charge position mentioned above.

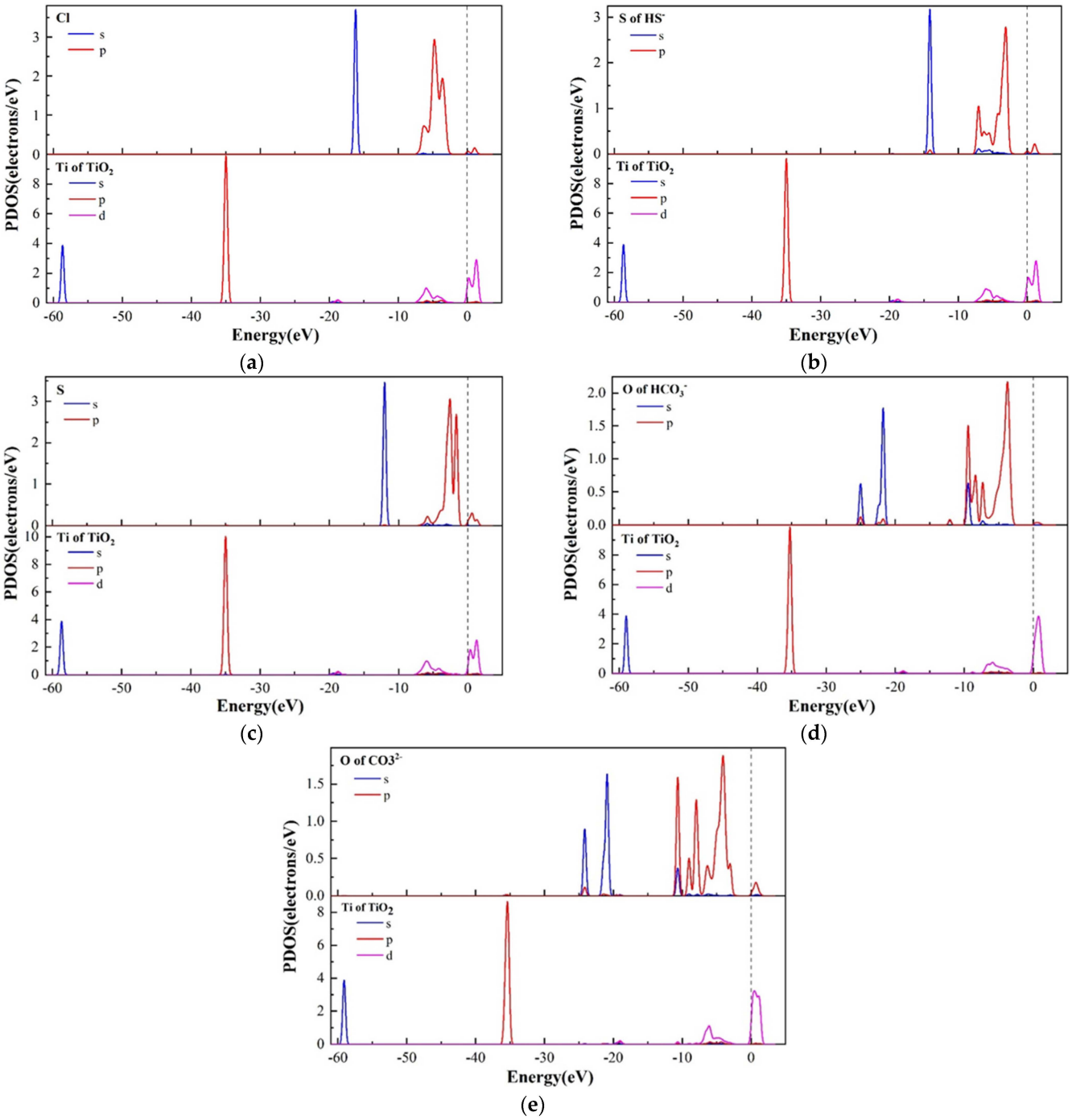

Figure 5. PDOS curves of corrosive species adsorbed on the bridge position of the TiO_2 (110) surface (note: the valence electrons of Cl, S, O and Ti are $3S^2 3P^5$, $3S^2 3P^4$, $2S^2 2P^4$ and $3p^6 3d^2 4s^2$, respectively): (**a**) Cl^-; (**b**) HS^-; (**c**) S^{2-}; (**d**) $HCO_3{}^-$; (**e**) $CO_3{}^{2-}$.

3.5. Interface Binding Energy

The stability of the interface can be quantitatively determined by the interface binding energy to determine the corrosion attack of corrosive species in the solution on metallic materials. The calculation equation of the interface binding energy is as follows [35]:

$$E_{\text{interface}} = E_{\text{t}} - (E_{\text{m}} + E_{\text{i}}) \quad (1)$$

where E_t is the total energy of the entire adsorption system after geometric optimization, E_m is the energy of the TiO_2 (110) system and E_i is the energy of the corrosive medium system (Cl^-, HS^-, S^{2-}, HCO_3^- and CO_3^{2-}).

Table 4 shows the final energies of the single Cl^-, HS^-, S^{2-}, HCO_3^-, CO_3^{2-} and TiO_2 (110) models after geometric optimization. The binding energies of the Cl^-, HS^-, $S^{2-}HCO_3^-$, CO_3^{2-} and TiO_2 (110) surfaces at bridge positions were obtained by Tables 2 and 4, as shown in Table 5. Table 5 shows that, compared with Cl^-, HS^-, HCO_3^- and CO_3^{2-}, it was easier for S^{2-} to bind and react with TiO_2, indicating that S^{2-} had strong adsorption on the TiO_2 (110) surface. The interface binding energy is an important parameter to characterize the interface thermodynamic stability; the smaller the value is, the more stable the interface structure is [35]. Therefore, the stability of TiO_2 in this environment containing S^{2-} was the poorest. The binding energy order of Cl^-, HS^-, S^{2-}, HCO_3^- and CO_3^{2-} with the TiO_2 (110) surface was $S^{2-} > CO_3^{2-} > Cl^- > HS^- > HCO_3^-$. The stability of TiO_2 in the environments containing Cl^-, HS^-, S^{2-}, HCO_3^- and CO_3^{2-} was $S^{2-} < CO_3^{2-} < Cl^- < HS^- < HCO_3^-$, which is in good accordance with the electron density results.

Table 4. Final energy of each corrosive species and TiO_2 (110) model after geometric optimization.

Model	Final Energy/eV
Cl^-	−411.7437852366
HS^-	−296.3156703881
S^{2-}	−280.4987150773
HCO_3^-	−1483.481392861
CO_3^{2-}	−1467.944344893
TiO_2 (110)	−29,766.99300605

Table 5. Interface binding energy between corrosive species and the bridge position of the TiO_2 (110) crystal face.

Model	Interfacial Binding Energy/eV
TiO_2 (bridge)—Cl^-	1.3756333366
TiO_2 (bridge)—HS^-	0.9833771481
TiO_2 (bridge)—S^{2-}	2.3614022773
TiO_2 (bridge)—HCO_3^-	0.382611491
TiO_2 (bridge)—CO_3^{2-}	1.927179543

4. Corrosion Mechanism

According to the above study, when corrosive ions (Cl^-, HS^-, S^{2-}, HCO_3^- and CO_3^{2-}) adsorbed on the TiO_2 (110) surface, their order of corrosion attack on the TiO_2 (110) surface was $S^{2-} > CO_3^{2-} > Cl^- > HS^- > HCO_3^-$. The corrosion resistance of TiO_2 in the environment containing H_2S was the worst, followed by CO_2, and the stability of TiO_2 in the environment containing Cl^- was better than the former two. In addition, the TC4 titanium alloy would suffer more serious corrosion in the CO_2-H_2S-Cl^- system due to the interaction between corrosive ions. The corrosion mechanism of the TC4 titanium alloy in the NaCl solution containing H_2S and CO_2 is shown in Figure 6.

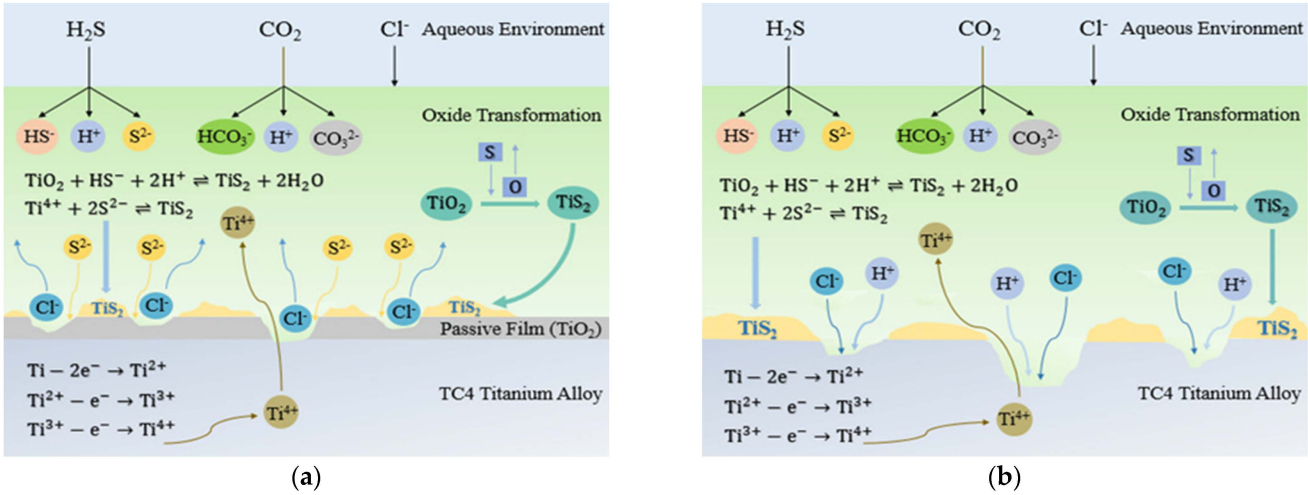

(**a**) (**b**)

Figure 6. Corrosion mechanism of the TC4 titanium alloy in the CO_2-H_2S-Cl^- system: (**a**) initial stage and (**b**) latter stage.

The following is the specific reaction process of each corrosive ion (Cl^-, HS^-, S^{2-}, HCO_3^- and CO_3^{2-}) on the passive film of the TC4 titanium alloy surface. The specific oxidation process of titanium is as follows [45,46]:

$$Ti - 2e^- \rightarrow Ti^{2+} \tag{2}$$

$$Ti^{2+} - e^- \rightarrow Ti^{3+} \tag{3}$$

$$Ti^{3+} - e^- \rightarrow Ti^{4+} \tag{4}$$

The total reaction equation is:

$$Ti^{2+} + O^{2-} \rightarrow TiO \tag{5}$$

$$2Ti^{3+} + 3O^{2-} \rightarrow Ti_2O_3 \tag{6}$$

$$Ti^{4+} + 2O^{2-} \rightarrow TiO_2 \tag{7}$$

The oxide film formed is mainly TiO_2. In the environment where titanium alloy is in service, H_2S will undergo an ionization reaction to ionize HS^-, S^{2-} and H^+, and the specific ionization process is as follows [47]:

$$2H_2S_{(aq)} \rightleftharpoons 2HS^- + 2H^+ \tag{8}$$

$$HS^-{}_{(aq)} \rightleftharpoons S^{2-} + H^+ \tag{9}$$

Obviously, the local concentration of HS^- increases with increasing sulfide concentrations, and the concentration of S^{2-} increases with increasing HS^- concentrations. The specific formation process of TiS_2 is mainly manifested in two situations [46]. The first one is shown in Equation (10), and the second one may be caused by chemical reaction after the electron transfer reaction. The specific reaction process is shown in Equation (11).

$$TiO_2 + HS^- + 2H^+ \rightleftharpoons TiS_2 + 2H_2O \tag{10}$$

$$Ti^{4+} + 2S^{2-} \rightleftharpoons TiS_2 \tag{11}$$

The corrosion of titanium alloy in a saturated CO_2 water environment is also electrochemical corrosion. CO_2 is dissolved in water to form H_2CO_3. After ionization, H_2CO_3 generates HCO_3^- and CO_3^{2-}. The specific reaction steps are as follows [47]:

$$CO_2 + H_2O \rightleftharpoons H_2CO_3 \tag{12}$$

$$H_2CO_3 \rightleftharpoons HCO_3^- + H^+ \quad (13)$$

$$HCO_3^- \rightleftharpoons CO_3^{2-} + H^+ \quad (14)$$

According to Equations (2)–(14) and the binding energy between the corrosive ions and the corrosive ions with the rutile TiO_2 (110) surface, when the initial corrosion system only contains the NaCl medium, Cl^- has a strong penetration, which can destroy the passive film TiO_2 on the titanium alloy surface. However, when H_2S and CO_2 are introduced into the system, although Cl^- has a superadsorption effect, the interfacial binding energy of Cl^- between TiO_2 is lower than those of S^{2-} and $CO_3{}^{2-}$, and the interfacial binding energy of S^{2-} between TiO_2 is higher than that of $CO_3{}^{2-}$. The literature showed that, in a corrosive environment where CO_2 and H_2S coexisted, the chemical adsorption capacity of HS^- was stronger than that of $HCO_3{}^-$ [48].

Therefore, S^{2-} will first exclude Cl^- and show a high concentration on the surface of the passive film. At this time, the damage of S^{2-} on the titanium alloy surface passive film TiO_2 is stronger than that of Cl^-. Therefore, TiO_2 firstly reacts with H_2S (or its hydrolysate) in the interface between the bulk solution and the metal matrix to form TiS_2. At the same time, HS^- and S^{2-} ionized by H_2S can promote the formation of TiS_2 compounds [45]. TiS_2 is mainly contained in the outer layer of the passive film. However, the source of some TiS_2 can be attributed to the competition of sulfur and oxygen for titanium bond orbitals, which is actually a central issue [49]. Since S and O are elements in the same main group, S more easily replaces O in passive film TiO_2. That is, the nucleation and growth of partial TiS_2 is a process of replacing Ti-O bonds with Ti-S bonds [49]. Some researchers believe that the formation of sulfides on metals is much faster than the formation of corresponding oxides [50].

When the formed corrosion scale TiS_2 is deposited on the substrate surface and reaches a certain saturation state, the formation of the corrosion scale TiS_2 gradually replaces the passive film TiO_2. At the moment, $CO_3{}^{2-}$ ionized from H_2CO_3 formed by CO_2 dissolved in water will act on TiO_2 to generate titanium carbonate. As a typical weak acid and alkali salt, titanium carbonate is easily hydrolyzed, but it will cause the dissolution of passive film or corrosion product film. Therefore, the existence of CO_2 will promote the dissolution of the TiS_2 film, destroy the structure of the TiS_2 film as well as the integrity of the passive film and corrosion scale and further erode the metal matrix.

H_2CO_3 formed by CO_2 dissolved in water provides a further acidified environment for Cl^- corrosion attack, resulting in a significant decrease in the stability of the passive film (or corrosion product film) in an acidic medium. At the same time, Cl^- itself has a corresponding influence on the formation of the corrosion product layer [51]. With the influence of H_2CO_3, Cl^- further destroys the integrity of TiS_2 on the metal matrix and accelerates the dissolution of the matrix [52], resulting in an increase in the number and depth of corrosion pits. The above discussion is consistent with the experimental results in the relevant literature: compared with the CO_2 corrosion environment in formation water, the passive film on the surface of titanium alloy is more vulnerable to damage in the water solution containing the H_2S corrosion medium [35]. Therefore, TC4 titanium alloy will suffer serious corrosion in the environment containing H_2S, followed by the environment containing CO_2, and it has relatively good corrosion resistance to Cl^-. When the corrosions H_2S, CO_2 and Cl^- coexist in the corrosion medium, TC4 titanium alloy will suffer more serious corrosion.

5. Conclusions

(1) The optimal adsorption positions of Cl^-, HS^-, S^{2-}, $HCO_3{}^-$ and $CO_3{}^{2-}$ on the surface of TiO_2 (110) were all bridge positions, followed by hole and top positions.

(2) When the corrosive ion adsorption on TiO_2 (110) reached a stable state, there was a strong charge interaction between the negatively charged Cl, S, O atoms in Cl^-, HS^-, S^{2-}, $HCO_3{}^-$ and $CO_3{}^{2-}$ and the positively charged Ti atoms in TiO_2. The bonding was caused by the transfer of the charge from around the Ti atom to around the Cl, O

and S atoms, forming the electron orbital hybridization of Cl-3p^5, S-3p^4, O-2p^4 and Ti-3d^2, and the adsorption mechanism was chemical adsorption.

(3) The binding energies of Cl^-, HS^-, S^{2-}, $HCO_3{}^-$ and $CO_3{}^{2-}$ with TiO_2 (110) were in the order of $S^{2-} > CO_3{}^{2-} > Cl^- > HS^- > HCO_3{}^-$. Titanium alloy would be corroded in the system containing S^{2-}, followed by $CO_3{}^{2-}$, Cl^-, HS^- and $HCO_3{}^-$, and the combined action of H_2S, CO_2 and Cl^- further accelerated the corrosion of titanium alloy.

Author Contributions: Conceptualization, P.D. and S.Z.; methodology, P.D. and Y.Z.; software, H.M.; validation, P.D.; formal analysis, Q.L.; investigation, Z.N.; data curation, J.L.; writing—original draft preparation, P.D.; writing—review and editing, S.Z. All authors have read and agreed to the published version of the manuscript.

Funding: This work was supported by the National Natural Science Foundation of China (51974245) and the Key Research and Development Program of Shaanxi Province (2022GY-128, 2022SF-045).

Data Availability Statement: Not applicable.

Acknowledgments: We thank the associate editor and the reviewers for their useful feedback that improved this paper, along with the Youth Innovation Team of Shaanxi University for the helpful discussions on topics related to this work.

Conflicts of Interest: The authors declare no conflict of interest. The funders had no role in the design of the study; in the collection, analyses or interpretation of data; in the writing of the manuscript; or in the decision to publish the results. All authors agreed to submit the manuscript to the journal.

References

1. Al-Moubaraki, A.H.; Obot, I.B. Top of the line corrosion: Causes, mechanisms, and mitigation using corrosion inhibitors. *Arab. J. Chem.* **2021**, *14*, 103116. [CrossRef]
2. Hou, B.R.; Li, X.G.; Ma, X.M.; Du, C.W.; Zhang, D.W.; Zheng, M.; Xu, W.C.; Lu, D.Z.; Ma, F.B. The cost of corrosion in China. *NPJ Mater. Degrad.* **2017**, *1*, 4. [CrossRef]
3. Wang, Z.Q.; Zhou, Z.Y.; Xu, W.C.; Yang, L.H.; Zhang, B.B.; Li, Y.T. Study on inner corrosion behavior of high strength product oil pipelines. *Eng. Fail. Anal.* **2020**, *115*, 104659. [CrossRef]
4. Stipaničev, M.; Turcu, F.; Esnault, L.; Schweitzer, E.W.; Kilian, R.; Basseguy, R. Corrosion behavior of carbon steel in presence of sulfate-reducing bacteria in seawater environment. *Electrochim. Acta* **2013**, *113*, 390–406. [CrossRef]
5. Xin, S.S.; Li, M.C. Electrochemical corrosion characteristics of type 316L stainless steel in hot concentrated seawater. *Corros. Sci.* **2014**, *81*, 390–406. [CrossRef]
6. Hoseinieh, S.M.; Homborg, A.M.; Shahrabi, T.; Mol, J.M.C.; Ramezanzadeh, B. A novel approach for the evaluation of under deposit corrosion in marine environments using combined analysis by electrochemical impedance spectroscopy and electrochemical noise. *Electrochim. Acta* **2016**, *217*, 226–241. [CrossRef]
7. Su, B.X.; Wang, B.B.; Luo, L.S.; Wang, L.; Su, Y.Q.; Wang, F.X.; Xu, Y.J.; Han, B.S.; Huang, H.G.; Guo, J.J.; et al. The corrosion behavior of Ti-6Al-3Nb-2Zr-1Mo alloy: Effects of HCl concentration and temperature. *J. Mater. Sci. Technol.* **2021**, *74*, 143–154. [CrossRef]
8. Tekin, K.C.; Malayoglu, U. Production of plasma electrolytic oxide coatings on Ti-6Al-4V alloy in aluminate-based electrolytes. *Surf. Eng.* **2017**, *33*, 787–795. [CrossRef]
9. Gai, X.; Bai, Y.; Li, J.; Li, S.J.; Hou, W.T.; Hao, Y.L.; Zhang, X.; Yang, R.; Misra, R.D.K. Electrochemical behaviour of passive film formed on the surface of Ti-6Al-4V alloys fabricated by electron beam melting. *Corros. Sci.* **2018**, *145*, 80–89. [CrossRef]
10. Seo, D.I.; Lee, J.B. Effects of competitive anion adsorption (Br^- or Cl^-) and semiconducting properties of the passive films on the corrosion behavior of the additively manufactured Ti-6Al-4V alloys. *Corros. Sci.* **2020**, *173*, 108789. [CrossRef]
11. Kaur, S.; Sharma, S.; Bala, N. A comparative study of corrosion resistance of biocompatible coating on titanium alloy and stainless steel. *Mater. Chem. Phys.* **2019**, *238*, 121923. [CrossRef]
12. Yang, Z.; Gu, H.; Sha, G.; Lu, W.J.; Yu, W.Q.; Zhang, W.J.; Fu, Y.F.; Wang, K.S.; Wang, L.Q. TC4/Ag metal matrix nanocomposites modified by friction stir processing: Surface characterization, antibacterial property, and cytotoxicity in vitro. *ACS Appl. Mater. Interfaces* **2018**, *10*, 41155–41166. [CrossRef] [PubMed]
13. Fazel, M.; Salimijazi, H.R.; Shamanian, M. Improvement of corrosion and tribocorrosion behavior of pure titanium by subzero anodic spark oxidation. *ACS Appl. Mater. Interfaces* **2018**, *10*, 15281–15287. [CrossRef]
14. Ren, S.; Du, C.W.; Liu, Z.Y.; Li, X.G.; Xiong, J.H.; Li, S.K. Effect of fluoride ions on corrosion behaviour of commercial pure titanium in artificial seawater environment. *Appl. Surf. Sci.* **2020**, *506*, 144759. [CrossRef]
15. Haldar, B.; Karmakar, S.; Saha, P.; Chattopadhyay, A.B. In situ multicomponent MMC coating developed on Ti–6Al–4V substrate. *Surf. Eng.* **2014**, *30*, 256–262. [CrossRef]

16. Tang, J.; Luo, H.Y.; Qi, Y.M.; Xu, P.W.; Ma, S.; Zhang, Z.; Ma, Y. The effect of cryogenic burnishing on the formation mechanism of corrosion product film of Ti-6Al-4V titanium alloy in 0.9% NaCl solution. *Surf. Coat. Technol.* **2018**, *345*, 123–131. [CrossRef]
17. Rahimipour, S.; Rafiei, B.; Salahinejad, E. Organosilane-functionalized hydrothermal-derived coatings on titanium alloys for hydrophobization and corrosion protection. *Prog. Org. Coat.* **2020**, *142*, 105594. [CrossRef]
18. Xing, H.R.; Hu, P.; Li, S.L.; Zuo, Y.G.; Han, J.Y.; Hua, X.J.; Wang, K.S.; Yang, F.; Feng, P.F.; Chang, T. Adsorption and diffusion of oxygen on metal surfaces studied by first-principle study: A review. *J. Mater. Sci. Technol.* **2021**, *62*, 180–194. [CrossRef]
19. Fu, D.L.; Guo, W.Y.; Liu, Y.J.; Chi, Y.H. Adsorption and dissociation of H_2S on $Mo_2C(001)$ surface-A first-principle study. *Appl. Surf. Sci.* **2015**, *351*, 125–134. [CrossRef]
20. Lin, L.; Yao, L.W.; Li, S.F.; Shi, Z.G.; Xie, K.; Zhu, L.H.; Tao, H.L.; Zhang, Z.Y. Effect of SiC(111) with different layers on adsorption properties of CO molecules. *Mater. Today Commun.* **2020**, *25*, 101596. [CrossRef]
21. Lin, L.; Yao, L.W.; Li, S.F.; Zhu, L.H.; Huang, J.T.; Wang, P.T.; Yu, W.Y.; He, C.Z.; Zhang, Z. The influence of SiC(111) surface with different layers on CH_4 adsorption. *Surf. Sci.* **2020**, *702*, 121699. [CrossRef]
22. Pantaroto, H.N.; Cordeiro, J.M.; Pereira, L.T.; de Almeida, A.B.; Junior, F.H.N.; Rangel, E.C.; Azevedo Neto, N.F.; da Silva, J.H.D.; Barão, V.A.R. Sputtered crystalline TiO_2 film drives improved surface properties of titanium-based biomedical implants. *Mater. Sci. Eng. C* **2021**, *119*, 111638. [CrossRef]
23. Mattsson, A.; Österlund, L. Adsorption and photoinduced decomposition of acetone and acetic acid on anatase, brookite, and rutile TiO_2 nanoparticles. *J. Phys. Chem. C* **2010**, *114*, 14121–14132. [CrossRef]
24. Cui, Y.Y.; Wang, Q.F.; Ren, J.S.; Liu, B.; Yang, G.; Gao, Y.F. Geometric and electronic properties of rutile TiO_2 with vanadium implantation: A first-principles calculation. *Nucl. Inst. Methods Phys. Res. B* **2019**, *455*, 35–38. [CrossRef]
25. Morgan, B.J.; Watson, G.W. A DFT+ U description of oxygen vacancies at the TiO_2 rutile (110) surface. *Surf. Sci.* **2007**, *601*, 5034–5041. (In Chinese) [CrossRef]
26. Burnside, S.D.; Shklover, V.; Barbé, C.; Comte, P.; Arendse, F.; Brooks, K.; Grätzel, M. Self-organization of TiO_2 nanoparticles in thin films. *Chem. Mater.* **1998**, *10*, 2419–2425. [CrossRef]
27. Wang, Y.; Huang, G.S. Adsorption of Au atoms on stoichiometric and reduced $TiO_2(110)$ rutile surfaces: A first principles study. *Surf. Sci.* **2003**, *542*, 72–80. [CrossRef]
28. Käckell, P.; Terakura, K. First-principle analysis of the dissociative adsorption of formic acid on rutile $TiO_2(110)$. *Appl. Surf. Sci.* **2000**, *166*, 370–375. [CrossRef]
29. Zhao, Y.F.; Ren, S.Y.; Wu, J.; Ji, Z.H.; Ma, Q.; Yang, M. Experimental study on the fabrication of TiO_2 phase-junction nanorods and deep removal of mercury from flue gas by photocatalyst. *J. Chin. Soc. Power Eng.* **2021**, *41*, 979–983+1018. [CrossRef]
30. Lin, L.; Shi, Z.G.; Yan, L.B.; Tao, H.L.; Yao, L.W.; Li, S.F.; Xie, K.; Huang, J.T.; Zhang, Z.Y. First-principles study of CO adsorption on Os atom doped anatase $TiO_2(101)$ surface. *Polyhedron* **2020**, *191*, 114814. [CrossRef]
31. Guo, Y.X.; Hu, R.M.; Zhou, X.L.; Yu, J.; Wang, L.H. A first principle study on the adsorption of H_2O_2 on CuO(111) and Ag/CuO(111) surface. *Appl. Surf. Sci.* **2019**, *479*, 989–996. [CrossRef]
32. Su, K.; Liu, D.M.; Pang, H.; Shao, T.M. Improvement on thermal stability of TiAlSiN coatings deposited by IBAD. *Surf. Eng.* **2018**, *34*, 504–510. [CrossRef]
33. Guo, W.B.; She, Z.Y.; Xue, H.T.; Zhang, X.M. Effect of active Ti element on the bonding characteristic of the Ag(111)/α-$Al_2O_3(0001)$ interface by using first principle calculation. *Ceram. Int.* **2020**, *46*, 5430–5435. [CrossRef]
34. Shi, Z.G.; Lin, L.; Chen, R.X.; Yan, L.B. Adsorption of CO molecules on anatase $TiO_2(001)$ loaded with noble metals M (M=Ir/Pd/Pt): A study from DFT calculations. *Mater. Today Commun.* **2021**, *28*, 102699. [CrossRef]
35. Li, Y.Y. Study on stability of titanium alloy passivation film under severe corrosion environment. *J. Xi'an Shiyou Univ. Nat. Sci. Ed.* **2018**, *33*, 120–126.
36. Wen, P.; Li, F.C.; Zhao, Y.; Zhang, F.C.; Tong, L.H. First principles calculation of occupancy, bonding characteristics and alloying effect of Cr, Mo, Ni in bulk alpha-Fe(C). *Acta Phys. Sin.* **2014**, *63*, 809. [CrossRef]
37. Mao, Y.L.; Hao, W.P.; Wei, X.L.; Yuan, J.M.; Zhong, J.X. Edge-adsorption of potassium adatoms on graphene nanoribbon: A first principle study. *Appl. Surf. Sci.* **2013**, *280*, 698–704. [CrossRef]
38. Yang, S.Q.; Liang, G.X.; Lv, M. First-principle study on adsorption energy and electronic characteristics of Ni plating interface. *Hot Work. Technol.* **2021**, *50*, 27–30. [CrossRef]
39. Li, W.; Lu, X.M.; Li, G.Q.; Ma, J.J.; Zeng, P.Y.; Chen, J.F.; Pan, Z.L.; He, Q.Y. First-principle study of SO_2 molecule adsorption on Ni-doped vacancy-defected single-walled (8,0) carbon nanotubes. *Appl. Surf. Sci.* **2016**, *364*, 560–566. [CrossRef]
40. Gao, X.; Zhou, Q.; Wang, J.X.; Xu, L.N.; Zeng, W. Adsorption of SO_2 molecule on Ni-doped and Pd-doped graphene based on first-principle study. *Appl. Surf. Sci.* **2020**, *517*, 146180. [CrossRef]
41. Lin, L.; Shi, Z.G.; Huang, J.T.; Wang, P.T.; Yu, W.Y.; He, C.Z.; Zhang, Z.Y. Molecular adsorption properties of CH_4 with noble metals doped onto oxygen vacancy defect of anatase $TiO_2(101)$ surface: First-principles calculations. *Appl. Surf. Sci.* **2020**, *514*, 145900. [CrossRef]
42. Ren, Y.J.; Du, H.Y.; Du, C.Y.; Chen, J.; Li, W.; Qiu, W.; Hsu, J.P.; Jiang, J.Z. Influence of oxygen adsorption on the chemical stability and conductivity of transition metal ceramic coatings: First-principle calculations. *Appl. Surf. Sci.* **2019**, *495*, 143530. [CrossRef]
43. Hu, Y.L.; Bai, L.H.; Tong, Y.G.; Deng, D.Y.; Liang, X.B.; Zhang, J.; Li, Y.J.; Chen, Y.X. First-principle calculation investigation of NbMoTaW based refractory high entropy alloys. *J. Alloys Compd.* **2020**, *827*, 153963. [CrossRef]

44. Luo, H.; Wang, D.Y.; Liu, L.X.; Li, L.C. Theoretical study on the adsorption characteristics of trichlorophenol on TiO_2(101) surface. *J. At. Mol. Phys.* **2020**, *37*, 349–353.
45. Yang, X.J.; Du, C.W.; Wan, H.X.; Liu, Z.Y.; Li, X.G. Influence of sulfides on the passivation behavior of titanium alloy TA_2 in simulated seawater environments. *Appl. Surf. Sci.* **2018**, *458*, 198–209. [CrossRef]
46. Wei, B.X.; Pang, J.Y.; Xu, J.; Sun, C.; Zhang, H.W.; Wang, Z.Y.; Yu, C.K.; Ke, W. Microbiologically influenced corrosion of TiZrNb medium-entropy alloys by Desulfovibrio desulfuricans. *J. Alloys Compd.* **2021**, *875*, 160020. [CrossRef]
47. Gong, Q.J.; Xiang, Y.; Zhang, J.Q.; Wang, R.T.; Qin, D.H. Influence of elemental sulfur on the corrosion mechanism of X80 steel in supercritical CO_2-saturated aqueous phase environment. *J. Supercrit. Fluids* **2021**, *176*, 105320. [CrossRef]
48. Wang, Y.; Wang, B.; He, S.; Zhang, L.; Xing, X.J.; Li, H.X.; Lu, M.X. Unraveling the effect of H_2S on the corrosion behavior of high strength sulfur-resistant steel in $CO_2/H_2S/Cl^-$ environments at ultra high temperature and high pressure. *J. Nat. Gas Sci. Eng.* **2022**, *100*, 104477. [CrossRef]
49. Li, Y.F.; Singh, A.; Reidy, K.; Jo, S.S.; Ross, F.M.; Jaramillo, R. Making large-area titanium disulfide films at reduced temperature by balancing the kinetics of sulfurization and roughening. *Adv. Funct. Mater.* **2020**, *30*, 2003617. [CrossRef]
50. Mantha, D.; Wen, X.; Reddy, R.G. High temperature oxidation of a Ti_3Al alloy in argon-5% SO_2 environment. *High Temp. Mater. Processes* **2004**, *23*, 93–102. [CrossRef]
51. Wei, B.X.; Chen, C.J.; Xu, J.; Yang, L.L.; Jia, Y.X.; Du, Y.; Guo, M.X.; Sun, C.; Wang, Z.Y.; Wang, F.H. Comparing the hot corrosion of (100), (210) and (110) Ni-based superalloys exposed to the mixed salt of Na_2SO_4-NaCl at 750 °C: Experimental study and first-principles calculation. *Corros. Sci.* **2022**, *195*, 109996. [CrossRef]
52. Qin, M.; Liao, K.X.; He, G.X.; Huang, Y.J.; Wang, M.N.; Zhang, S.J. Main control factors and prediction model of flow-accelerated CO_2/H_2S synergistic corrosion for X65 steel. *Process Saf. Environ. Prot.* **2022**, *160*, 749–762. [CrossRef]